Int. J. Nanoelectronics and Materials **1** (2008) 53-64

Study of intersubband transitions in $Si_{1-x}Ge_x/Si$ quantum wells using 14-band k·p model

W. Liu[1], D. H. Zhang[1,*], T. H. Loh[2], W.J. Fan[1], S.F. Yoon[1], N. Balasubramanian[2]

[1]) *School of Electrical and Electronic Engineering, Nanyang Technological University, Singapore 639798.*
[2]) *Institute of Microelectronics, 11 Science Park Road , Singapore Science Park II, Singapore 117685.*

Abstract

Optical intersubband transitions (ISTs) for both in-plane polarization (TE) and normal-to-plane polarization (TM) in p-type $Si_{1-x}Ge_x/Si$ multiple quantum wells (MQWs) are investigated using 14-band **k·p** model combined with the envelope-function Fourier expansion method. The results show that the amplitudes of different intersubband transitions for TE and TM polarizations, and the overall absorption vary regularly with the well width as it affects the distribution of bound and continuum excited states directly, and TE mode absorption dominates in all the QWs studied. This work provides useful information for design and analysis of $Si_{1-x}Ge_x/Si$ quantum well infrared photodetectors (QWIPs).

1. Introduction

Quantum well infrared photodetectors (QWIPs) are an important technology for infrared imaging and sensing, offering the advantages of mature material growth technology, good uniformity, high quantum efficiency and high detectivity.[1-3] The n-type QWIPs which are most widely studied require coupling gratings to change the incident light direction due to their inability to absorb normal incident light. As an alternative approach, p-type QWIPs allow detection of normal incident light due to the intermixing of heavy-hole (HH), light-hole (LH) and spin-orbit splitting (SO) bands.[4-6] The p-type $Si_{1-x}Ge_x/Si$ QWIPs are attractive since they are compatible to the current Si microelectronics techniques, and can be monolithically integrated to fabricate large detector arrays with a CMOS readout circuitry.[7-11] Over the recent years there have been some experimental reports on normal-incidence photodetection in mid-wavelength (3-5 μm) and long-wavelength (8-14 μm) infrared atmosphere windows by intervalence-subband transitions of $Si_{1-x}Ge_x/Si$ quantum wells (QWs).[7-11] Some theoretical

*) For correspondence, E-mail: edhzhang@ntu.edu.sg, Tel: + 65 67904841.

work has also been done to study the underlying physics and calculate the dispersion of valance subbands of $Si_{1-x}Ge_x/Si$ QWIPs, such as pseudopotential mehod and 6-band **k·p** method that consider the coupling of HH, LH and SO into account.[12,13] Furthermore, Ridene *et al.* have investigated the infrared intersubband transitions (ISTs) in SiGe/Si QWs using 14-band **k·p** Hamiltonian that takes both the *p*-like first conduction and the *s*-like second conduction band into consideration and compare the results with those using 8-band and 12-band **k·p** Hamiltonians, showing that the *p*-*p* interaction favors the transition for in-plane (TE) polarized light.[14] In this article, we employ 14-band **k·p** model combined with the envelope-function Fourier expansion method to further analyze the variation of ISTs for TE (in-plane) and TM (normal-to-plane) polarizations with well width which affects the dispersion of valence subbands directly and in turn the characteristics of both TE and TM polarized ISTs.

2. Methods

The 14-band **k·p** Hamiltonian is given by

$$H = \begin{bmatrix} H_{pc} & H_{pc-s,pv} \\ (6\times 6) & (6\times 8) \\ H^{*}_{pc-s,pv} & H_{s,pv} \\ (8\times 6) & (8\times 8) \end{bmatrix}, \tag{1}$$

where the matrix H_{pc} consists of the elements of the six *p*-like conduction band states, the matrix $H_{s,pv}$ consists of the elements of the two *s*-like conduction band states and the six *p*-like valence band states, $H_{pc-s,pv}$ consists of the elements coupling the *p*-like conduction bands with the *s*-like conduction bands and *p*-like valence bands, and $H^{*}_{pc-s,pv}$ at the down triangular block consists of the corresponding conjugation elements of $H_{pc-s,pv}$. The details of H_{pc}, $H_{s,pv}$ and $H_{pc-s,pv}$ are listed in APPENDIX A. The strain Hamiltonian H_s can be derived by the following substitution because of the same underlying symmetry: $A \to a_v$, $B \to b$, $D \to d$, $k_\alpha k_\beta \to \varepsilon_{\alpha\beta}$ ($\alpha, \beta = x, y, z$), and $\hbar^2 k^2 / 2m_0 \leftrightarrow a_c$ for conduction band, where $\varepsilon_{\alpha\beta}$ is the strain tensor, *b* and *d* are the shear deformation potentials, a_v is the hydrostatic valence-band deformation potential, and a_c is the conduction-band deformation potential.

In the 14-band scheme, the total wave function of the subband *n* in QW can be written as

$$\Psi_n(r) = \sum_{j=1}^{14} F_{n,j}(r) u_{n,j}(r) \tag{2}$$

where $F_j(r)$ are the envelope functions and $u_j(r)$ are the periodic part of the Bloch basis functions at the zone center. The Bloch functions $u_j(r)$ we used are listed below

$$
\begin{aligned}
u_1 &= \phi_{HE,\alpha} = -i\sqrt{1/2}\left|(X_c + iY_c)\uparrow\right\rangle, \\
u_2 &= \phi_{LE,\alpha} = i\sqrt{2/3}\left|Z_c\uparrow\right\rangle - i\sqrt{1/6}\left|(X_c + iY_c)\downarrow\right\rangle, \\
u_3 &= \phi_{LE,\beta} = i\sqrt{2/3}\left|Z_c\downarrow\right\rangle + i\sqrt{1/6}\left|(X_c - iY_c)\uparrow\right\rangle, \\
u_4 &= \phi_{HE,\beta} = i\sqrt{1/2}\left|(X_c - iY_c)\downarrow\right\rangle, \\
u_5 &= \phi_{SOE,\alpha} = i\sqrt{1/3}\left|Z_c\uparrow\right\rangle + i\sqrt{1/3}\left|(X_c + iY_c)\downarrow\right\rangle, \\
u_6 &= \phi_{SOE,\beta} = -i\sqrt{1/3}\left|Z_c\downarrow\right\rangle + i\sqrt{1/3}\left|(X_c - iY_c)\uparrow\right\rangle, \\
u_7 &= \phi_{C,\alpha} = \left|S\uparrow\right\rangle, \\
u_8 &= \phi_{C,\beta} = \left|S\downarrow\right\rangle, \\
u_9 &= \phi_{HH,\alpha} = -i\sqrt{1/2}\left|(X_v + iY_v)\uparrow\right\rangle, \\
u_{10} &= \phi_{LH,\alpha} = i\sqrt{2/3}\left|Z_v\uparrow\right\rangle - i\sqrt{1/6}\left|(X_v + iY_v)\downarrow\right\rangle, \\
u_{11} &= \phi_{LH,\beta} = i\sqrt{2/3}\left|Z_v\downarrow\right\rangle + i\sqrt{1/6}\left|(X_v - iY_v)\uparrow\right\rangle, \\
u_{12} &= \phi_{HH,\beta} = i\sqrt{1/2}\left|(X_v - iY_v)\downarrow\right\rangle, \\
u_{13} &= \phi_{SOH,\alpha} = i\sqrt{1/3}\left|Z_v\uparrow\right\rangle + i\sqrt{1/3}\left|(X_v + iY_v)\downarrow\right\rangle, \\
u_{14} &= \phi_{SOH,\beta} = -i\sqrt{1/3}\left|Z_v\downarrow\right\rangle + i\sqrt{1/3}\left|(X_v - iY_v)\uparrow\right\rangle,
\end{aligned} \tag{3}
$$

where $|S\rangle$ indicates the *s*-like conduction band Bloch state, $|X_c\rangle$, $|Y_c\rangle$ and $|Z_c\rangle$ indicate the *p*-like conduction band Bloch states, and $|X\rangle$, $|Y\rangle$ and $|Z\rangle$ indicate the *p*-like valence band Bloch states. HH (heavy hole), LH (light hole) and SOH (spin-orbit splitting) denote the three states of the *p*-like valence band, respectively. HE (heavy electron), LE (light electron) and SOE (spin-orbit splitting) denote the three states of the *p*-like conduction band, respectively. C denotes the s-like conduction band state.

The three momentum matrix elements are defined as

$$P_0 = i\langle S|p_x|X_v\rangle = i\langle S|p_y|Y_v\rangle = i\langle S|p_z|Z_v\rangle, \tag{4}$$

$$P_1 = i\langle S|p_x|X_c\rangle = i\langle S|p_y|Y_c\rangle = i\langle S|p_z|Z_c\rangle, \tag{5}$$

$$
\begin{aligned}
Q &= i\langle X_c|p_z|Y_v\rangle = i\langle X_c|p_y|Z_v\rangle = i\langle Z_c|p_x|Y_v\rangle \\
&= -i\langle X_v|p_z|Y_c\rangle = -i\langle X_v|p_y|Z_c\rangle = -i\langle Z_v|p_x|Y_c\rangle
\end{aligned}, \tag{6}
$$

where P_0 is the coupling of *s*-like conduction band and *p*-like valence band, P_1 is the coupling of *p*-like conduction band and *s*-like conduction band, and Q is the coupling of *p*-like conduction band and *p*-like valence band.

The envelope-function Fourier expansion method [15-17] in QWs was employed here. The expansion takes the form of

$$F_{n,j}(r) = \exp[i(k_x x + k_y y)]\sum_m a_{n,j,m}\phi_m(z), \tag{7}$$

where
$$\phi_m(z) = \frac{1}{\sqrt{L}} \exp\left[i\left(k_z + m \cdot \frac{2\pi}{L} \right) \cdot z \right], \tag{8}$$

m is an integral denoting the order of related expansion term, $L = L_W + L_B$ is the structural period of QWs, where L_W and L_B are the well and barrier widths, respectively. This discrete Fourier series assumes that the overall structure is periodic with period L along the growth direction. In the case of multiple quantum wells (MQWs) which are employed in QWIPs and quantum cascade lasers (QCLs) mostly, this is exactly what's wanted.

Each subband calculated in the QWs consists of the components of all the 14 bands actually. The following probability functions are introduced to decide the HH, LH, SOH, C, HE, LE, and SOE components in the QW energy states:

$$\begin{aligned}
P_n^{HE} &= \sum_{j=1,4} \sum_m a^*_{n,j,m} a_{n,j,m} \ , \ P_n^{LE} = \sum_{j=2,3} \sum_m a^*_{n,j,m} a_{n,j,m} \ , \\
P_n^{SOE} &= \sum_{j=5,6} \sum_m a^*_{n,j,m} a_{n,j,m} \ , \ P_n^{CB} = \sum_{j=7,8} \sum_m a^*_{n,j,m} a_{n,j,m} \ , \\
P_n^{HH} &= \sum_{j=9,12} \sum_m a^*_{n,j,m} a_{n,j,m} \ , \ P_n^{LH} = \sum_{j=10,11} \sum_m a^*_{n,j,m} a_{n,j,m} \ , \\
P_n^{SOH} &= \sum_{j=13,14} \sum_m a^*_{n,j,m} a_{n,j,m} \ ,
\end{aligned} \tag{9}$$

where n denotes the QW subband index. These probability functions are particularly useful in identifying the dominant character in a particular subband. Note that the following sum rule should hold:

$$\sum_i P_n^i = 1 \qquad i = HE, LE, SOE, CB, HH, LH, SOH, . \tag{10}$$

The momentum matrix element between subband n and n' is

$$M_{nn'} = \left\langle \Psi_n \middle| \hat{e} \cdot \mathbf{p} \middle| \Psi_{n'} \right\rangle = \sum_{j,j'=1}^{8} \left\langle F_{nj} u_j \middle| \hat{e} \cdot \mathbf{p} \middle| F_{n'j'} u_{j'} \right\rangle \tag{11}$$

where $\hat{e} = \nu_x e_x + \nu_y e_y + \nu_z e_z \ \ (\nu_x^2 + \nu_y^2 + \nu_z^2 = 1)$ is the photon polarization unit vector.

Substituting (7) into (11), one can obtain

$$\begin{aligned}
M_{nn'} &= \sum_{j,j'=1}^{8} \left\langle \sum_m a_{n,j,m} \phi_m(z) u_j \middle| \hat{e} \cdot \mathrm{p} \middle| \sum_{m'} a_{n',j',m'} \phi_{m'}(z) u_{j'} \right\rangle \\
&= \sum_{j,j'=1}^{8} \left[\left\langle \sum_m a_{n,j,m} \phi_m(z) \middle| \hat{e} \cdot \mathrm{p} \middle| \sum_{m'} a_{n',j',m'} \phi_{m'}(z) \right\rangle \left\langle u_j \middle| u_{j'} \right\rangle \right] \\
&\quad + \sum_{j,j'=1}^{8} \left[\left\langle \sum_m a_{n,j,m} \phi_m(z) \middle| \sum_{m'} a_{n',j',m'} \phi_{m'}(z) \right\rangle \left\langle u_j \middle| \hat{e} \cdot \mathrm{p} \middle| u_{j'} \right\rangle \right]
\end{aligned} \tag{12}$$

Since $\left\langle u_j \middle| u_{j'} \right\rangle = \delta_{jj'}$ and $\left\langle \phi_m(z) \middle| \phi_{m'}(z) \right\rangle = \delta_{mm'}$, Eq. (12) becomes

$$M_{nn'} = \sum_{j=1}^{8}\left[\left\langle \sum_{m} a_{n,j,m}\phi_m(z)\left|\hat{e}\cdot \mathrm{p}\right|\sum_{m'} a_{n',j,m'}\phi_{m'}(z)\right\rangle\right] + \sum_{j,j'=1}^{8}\left[\sum_{m}\left(a^{*}_{n,j,m}\cdot a_{n',j',m}\right)\left\langle u_j\left|\hat{e}\cdot \mathrm{p}\right|u_{j'}\right\rangle\right] \tag{13}$$

where the first term on the right of Eq. (13) is the transitions within the same Bloch basis states (intraband contribution), and the second term on the right of Eq. (13) is the transitions between $|S\rangle$ and $|\nu\rangle$ ($|\nu\rangle$=$|X\rangle$, $|Y\rangle$ or $|Z\rangle$) states (interband contribution).

After deriving $M_{nn'}$, the absorption coefficient between subband n and n' can then be calculated by [18]

$$\alpha_{nn'}(\hbar\omega) = \frac{\pi e^2}{n_r c\varepsilon_0 m_0^2 \omega}\frac{2}{V}\sum_{k_t}\left|M_{nn'}\right|^2 \delta(E_{n'} - E_n - \hbar\omega)(f_n - f_{n'}) \tag{14}$$

where f_n and $f_{n'}$ are the Fermi-Dirac distributions for electrons in the subbands, k_t is the in-plane wave vector. In calculations the scattering relaxation should be taken into consideration and therefore the delta function in Eq. (14) should be replaced by a Lorentzian function with linewidth Γ as follows

$$\delta(E_{n'} - E_n - \hbar\omega) \to \frac{\Gamma/(2\pi)}{(E_{n'} - E_n - \hbar\omega)^2 + (\Gamma/2)^2} \tag{15}$$

3. Results and discussions

We choose $Si_{0.75}Ge_{0.25}$/Si MQW structures in the calculation as they can detect long wavelength infrared. A heavy-hole valence band offset of $\Delta E_V = 840x$ meV has been assumed.[19] The basic material parameters of Si and Ge are taken from Ref. 20. The in-plane strains are assumed to be $e_{xx} = (a - a_0)/a_0$, where a and a_0 are the after-strained and before-strained lattice constants, respectively. The strain at the perpendicular direction is $e_{zz} = -2(c_{12}/c_{11})e_{xx}$, where c_{11} and c_{12} is the elastic stiffness constants.

Figure 1 shows the calculated valence subband energy dispersions along [110] direction for the QW with different well widths (L_W). The lowest four hole subbands (H1-H4) are displayed in the figures. The barrier width is assumed to be 50 nm. It can be seen that all the subbands move upwards gradually with the increase of well width. The strong nonparabolic energy dispersion of each subband indicates serious band intermixing.

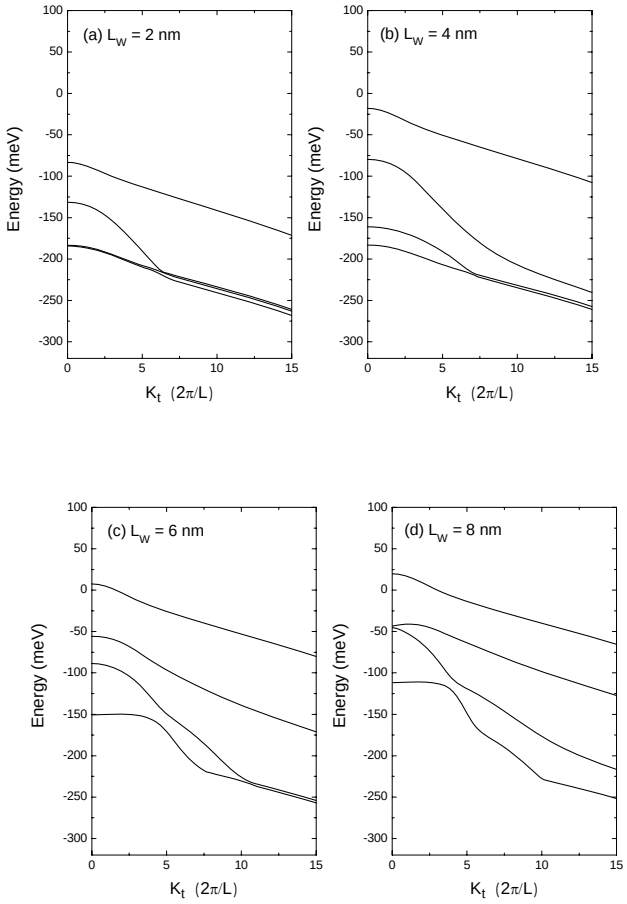

Fig. 1: Valence Subband energy dispersions along [110] direction of $Si_{0.75}Ge_{0.25}/Si$ MQWs with well widths of (a)
2nm, (b) 4 nm, (c) 6 nm and (d) 8 nm, respectively. The Si barrier width is assumed to be 50 nm.

The distribution of HH, LH and SO components in the four valence subbands as a function of k_t calculated using Eq. (9) for the $Si_{0.75}Ge_{0.25}/Si$ MQW with well width of 4 nm is shown in Fig. 2 to account for the intermixing effect. It is seen that the dominant components at the zone center ($k_t = 0$) are HH, LH, HH and HH for subbands H1-H4, respectively. However, strong intermixing appears when $k_t \neq 0$ and so each subband consists of comparable components of HH, LH and SO bands.

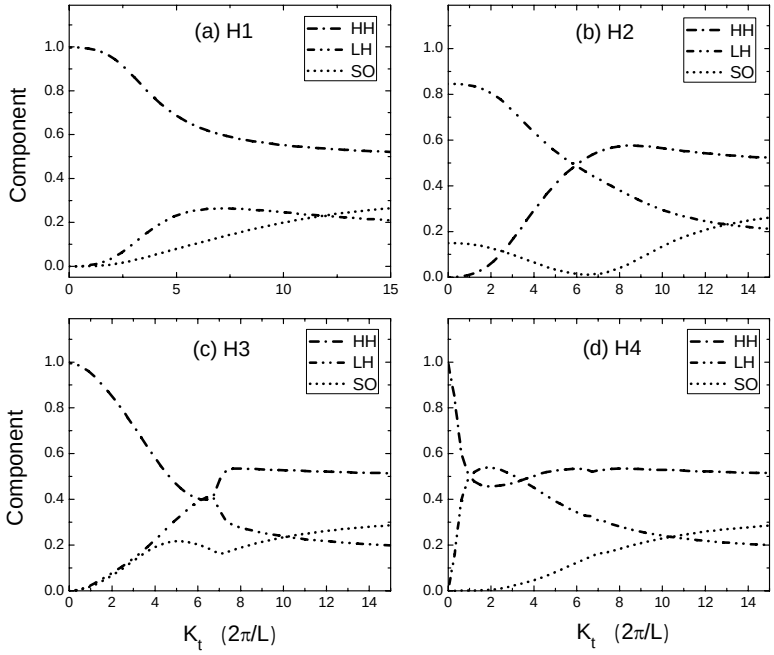

Fig. 2: Calculated compositions of HH, LH and SO in the lowest four valence subbands, H1, H2, H3 and H4, as a function of k_t for the $Si_{0.75}Ge_{0.25}$/Si MQW with a well width of 4 nm.

Figures 3 and 4 show the calculated squared optical transition matrix elements $Q_{TE(TM)}$ as a function of the in-plane wave vector for both TE and TM polarizations for the SiGe/Si MQW with well widths of 4 nm and 8 nm, respectively. Note that the relation between $Q_{TE(TM)}$ and the momentum matrix element $M_{TE(TM)}$ is $Q_{TE(TM)} = 2\left|M_{TE(TM)}\right|^2 / m_0$. It can be seen that in the case of 4 nm well width, H1-H2 transition is dominant in the TE polarized ISTs, and H1-H2 and H1-H3 transitions are dominant in the TM polarized ISTs. The calculated result for 2 nm well width shows similar pattern except only H1-H2 transition is dominant in the TM polarized ISTs. However, when the well width increases to 6 nm and 8 nm, H1 to H2, H3 and H4 transitions have comparable amplitudes for both TE and TM polarized ISTs.

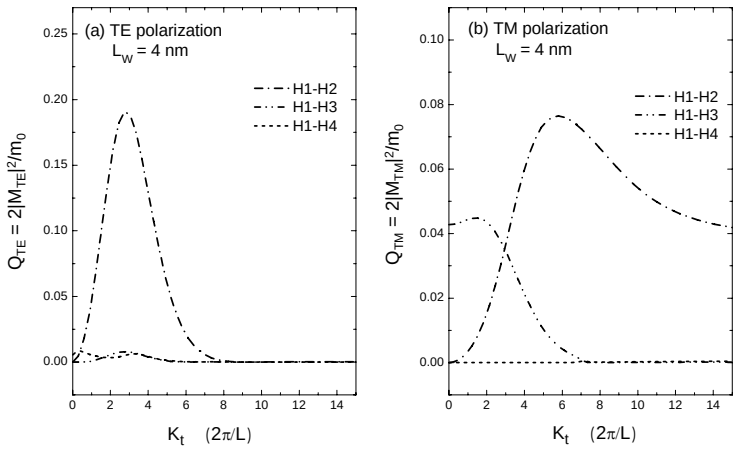

Fig. 3: Calculated squared optical transition matrix elements as a function of k_t along [110] direction of H1 to H2-H4 transitions for (a) TE polarization (Q_{TE}) and (b) TM polarization (Q_{TM}) for the $Si_{0.75}Ge_{0.25}/Si$ MQWs with a well width of 4 nm.

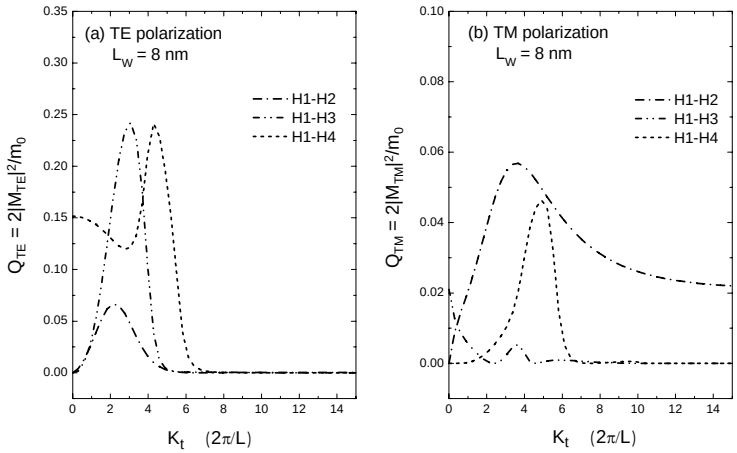

Fig. 4: Calculated squared optical transition matrix elements as a function of k_t of H1 to H2-H4 transitions for (a) TE polarization (Q_{TE}) and (b) TM polarization (Q_{TM}) for the $Si_{0.75}Ge_{0.25}/Si$ MQWs with well width of 8 nm.

Furthermore, the optical absorption coefficients as a function of photon energy for the QW with different well widths are computed and the results for both TE and TM polarizations are shown in Fig. 5. The linewidth Γ in the Lorentzian function Eq. (15) is assumed to be 18 meV in the calculation.[16] The calculated absorption coefficient has been normalized to one QW period. In the case of 2nm well width, either TE or TM absorption curve shows only one peak that comes from H1-H2 transition mainly while the other transitions are negligible. In the case of 4 nm well width, the TE absorption peak at 62.2 meV is due to H1-H2 transition,

and the TM absorption peaks at 66.6 and 137.2 meV are due to H1-H2 and H1-H3 transitions, respectively. When the well width increases to 6 nm, three peaks appear in both TE and TM absorption curves. The TE absorption peaks at 60.9, 98.9 and 151.2 meV are from H1 to H2, H3 and H4 transitions, respectively. The TM absorption peaks at 65.0, 94.7 and 137.7 meV are from H1 to H2, H3 and H4 transitions, respectively. When the well width increases further to 8 nm, the TE and TM absorption curves show similar patterns. It is clearly seen that although both TE and TM absorptions exist in the QW with 4 different well width, the TE absorption, however, dominate in all cases.

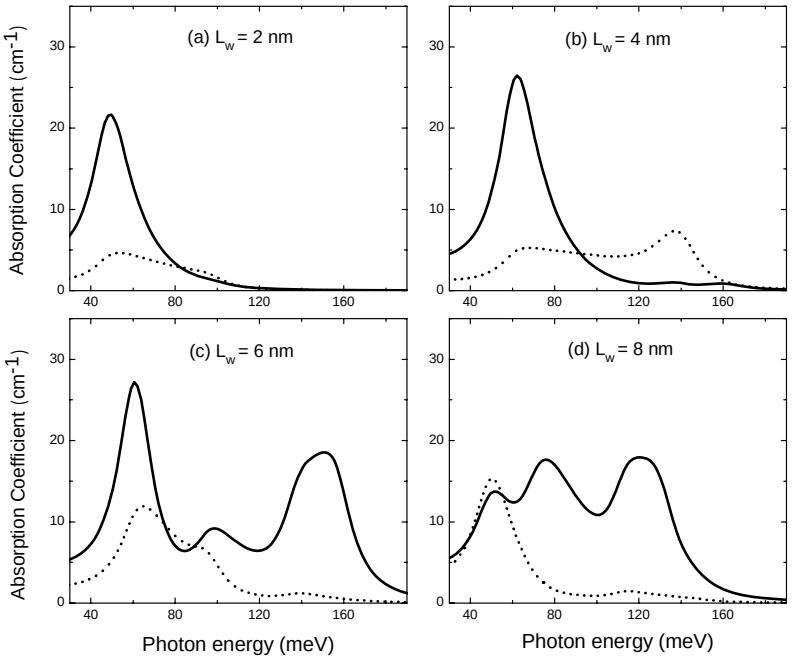

Fig. 5: Calculated optical absorption coefficients as a function of photon energy for the $Si_{0.75}Ge_{0.25}$/Si with well widths of (a) 2 nm, (b) 4 nm, (c) 6 nm and (d) 8 nm, respectively. The solid lines show the absorption for TE polarization and the dash lines show the absorption for TM polarization.

It's indicated that the ISTs in the valence band are always dominated by the transitions from the ground state to lower bound excited states. In the case of narrower wells only H1 and H2 are fairly bound states, so H1-H2 absorption is much greater than the others. In the case of broader wells where H3 and H4 become fairly bound states, H1-H3 and H1-H4 absorptions become comparable to H1-H2 absorption. However, there is no apparent selectivity appearing in different bound-bound state transitions for either TE or TM polarizations, because of the strong intermixing of HH, LH and SO in each valence subband as shown in Fig.2.

As far as the wavelength is concerned, the QW with 2 nm and 4 nm well widths, the absorption peaks at about 25 μm and 20 μm, respectively. For the QW with a 6 nm well, there are two significant absorption peaks at about 20 μ and 9 μm, respectively, which can be used

as two color detectors. For the QW with a well of 8 nm, although it shows 3 absorption peaks at about 20 μm, 16 μm and 10 μm respectively, the QW can be a better detector for a wide spectrum band.

4. CONCLUSIONS

In conclusion, we have used 14-band **k·p** model combined with the envelope-function Fourier expansion method to analyze the dependence of ISTs in p-type $Si_{1-x}Ge_x/Si$ MQWs on the well width. It's found that the transitions from the ground state H1 to the lower bound states are dominating for both TE and TM polarized absorptions and TE absorption dominates in all the QWs studied. Consequently, the amplitudes of different intersubband transitions, and therefore the overall absorption, would vary with well width which affects the distribution of bound and continuum excited states directly. With this method, one can easily design detectors with required peak wavelength and linewidth.

Appendix A: H_{pc}, $H_{s,pv}$ and $H_{pc\text{-}s,pv}$

The elements of H_{pc}, $H_{s,pv}$ and $H_{pc\text{-}s,pv}$ in the 14-band **k·p** Hamiltonian H (Eq. 6) are given by

$$H_{pc}=\begin{bmatrix} E_{g2}+F_c & H_c & I_c & 0 & \frac{H_c}{\sqrt{2}} & \sqrt{2}I_c \\ \cdots & E_{g2}+G_c & 0 & I_c & \frac{G_c-F_c}{\sqrt{2}} & -\sqrt{\frac{3}{2}}H_c \\ \cdots & \cdots & E_{g2}+G_c & -H_c & -\sqrt{\frac{3}{2}}H_c^* & -\frac{G_c-F_c}{\sqrt{2}} \\ \cdots & \cdots & \cdots & E_{g2}+F_c & -\sqrt{2}I_c^* & \frac{H_c^*}{\sqrt{2}} \\ \cdots & \cdots & \cdots & \cdots & E_{g2}+\frac{F_c+G_c}{2}-\Delta_c & 0 \\ \cdots & \cdots & \cdots & \cdots & \cdots & E_{g2}+\frac{F_c+G_c}{2}-\Delta_c \end{bmatrix}, \quad \text{(A1)}$$

$$H_{pc-s,pv}=\begin{bmatrix} -p_1k_- & 0 & 0 & \sqrt{\frac{2}{3}}qk_+ & \frac{1}{\sqrt{3}}qk_z & 0 & \frac{1}{\sqrt{3}}qk_+ & \frac{2}{\sqrt{3}}qk_+ \\ \sqrt{\frac{2}{3}}p_1k_z & \frac{-1}{\sqrt{3}}p_1k_- & -\sqrt{\frac{2}{3}}qk_- & 0 & 0 & \frac{1}{\sqrt{3}}qk_z & 0 & -qk_+ \\ \frac{1}{\sqrt{3}}p_1k_+ & \sqrt{\frac{2}{3}}pk_z & -\frac{1}{\sqrt{3}}qk_z & 0 & 0 & -\sqrt{\frac{2}{3}}qk_+ & qk_- & 0 \\ 0 & p_1k_+ & 0 & -\frac{1}{\sqrt{3}}qk_z & \sqrt{\frac{2}{3}}qk_- & 0 & \sqrt{\frac{2}{3}}qk_z & -\frac{1}{\sqrt{3}}qk_- \\ \frac{1}{\sqrt{3}}p_1k_z & \sqrt{\frac{2}{3}}p_1k_- & -\frac{1}{\sqrt{3}}qk_- & 0 & -qk_+ & -\sqrt{\frac{2}{3}}qk_z & 0 & 0 \\ \sqrt{\frac{2}{3}}p_1k_+ & \frac{-1}{\sqrt{3}}pk_z & -\sqrt{\frac{2}{3}}qk_z & qk_- & 0 & \frac{1}{\sqrt{3}}qk_+ & 0 & 0 \end{bmatrix} \quad \text{(A2)}$$

$$H_{s,pv}=\begin{bmatrix} E_g+\frac{\hbar^2k^2}{2m_0} & 0 & -p_0k_+ & \sqrt{\frac{2}{3}}p_0k_z & \frac{1}{\sqrt{3}}p_0k_- & 0 & \frac{1}{\sqrt{3}}p_0k_z & \sqrt{\frac{2}{3}}p_0k_- \\ \cdots & E_g+\frac{\hbar^2k^2}{2m_0} & 0 & \frac{-1}{\sqrt{3}}p_0k_+ & \sqrt{\frac{2}{3}}p_0k_z & p_0k_- & \sqrt{\frac{2}{3}}p_0k_+ & \frac{-1}{\sqrt{3}}p_0k_z \\ \cdots & \cdots & F & H & I & 0 & \frac{H}{\sqrt{2}} & \sqrt{2}I \\ \cdots & \cdots & \cdots & G & 0 & I & \frac{1}{\sqrt{2}}(G-F) & -\sqrt{\frac{3}{2}}H \\ \cdots & \cdots & \cdots & \cdots & G & -H & -\sqrt{\frac{3}{2}}H^* & \frac{-1}{\sqrt{2}}(G-F) \\ \cdots & \cdots & \cdots & \cdots & \cdots & F & -\sqrt{2}I^* & \frac{H^*}{\sqrt{2}} \\ \cdots & \cdots & \cdots & \cdots & \cdots & \cdots & \frac{F+G}{2}-\Delta & 0 \\ \cdots & \cdots & \cdots & \cdots & \cdots & \cdots & \cdots & \frac{F+G}{2}-\Delta \end{bmatrix}$$

……(A3)

where

$$k_+=(k_x+ik_y)/\sqrt{2},\ k_-=(k_x-ik_y)/\sqrt{2},$$

$$F=Ak^2+\frac{B}{2}(k^2-3k_z^2),\ G=Ak^2-\frac{B}{2}(k^2-3k_z^2),$$

$$H=-Dk_z(k_x-ik_y),\ I=-\frac{\sqrt{3}}{2}B(k_x^2-k_y^2)+iDk_xk_y,$$

$$A=-\frac{\hbar^2\gamma_1}{2m_0},\ B=-\frac{\hbar^2\gamma_2}{m_0},\ D=-\sqrt{3}\frac{\hbar^2\gamma_3}{m_0},$$

$$F_c=A_ck^2+\frac{B_c}{2}(k^2-3k_z^2),\ G_c=A_ck^2-\frac{B_c}{2}(k^2-3k_z^2),$$

$$H_c=-D_ck_z(k_x-ik_y),\ I_c=-\frac{\sqrt{3}}{2}B_c(k_x^2-k_y^2)+iD_ck_xk_y,$$

$$A_c=-\frac{\hbar^2\gamma_{c1}}{2m_0},\ B=-\frac{\hbar^2\gamma_{c2}}{m_0},\ D=-\sqrt{3}\frac{\hbar^2\gamma_{c3}}{m_0},$$

$$p_0=(\hbar/m_0)\cdot P_0,\ p_1=(\hbar/m_0)\cdot P_1 \text{ and } q=(\hbar/m_0)\cdot Q. \qquad \text{(A4)}$$

where γ_1, γ_2, γ_3, γ_{c1}, γ_{c2} and γ_{c3} are the modified Luttinger parameters of the *p*-like valence and conduction bands. The down triangular block in matrices (A1) and (A3) are not shown since they are Hermitian.

References

[1] B. F. Levine, J. Appl. Phys. **74** (1993) R1
[2] H. C. Liu, C. Y. Song, A. J. Springthorpe, J. C. Cao, Appl. Phys. Lett. **84** (2004)4068
[3] Lin Jiang, Sheng S. Li, M. Z. Tidrow, W. R. Dyer, W. K. Liu, J. M. Fastenau, T. R. Yurasits, Appl. Phys. Lett. **79** (2001)2982
[4] B. F. Levine, S. D. Gunapala, J. M. Kuo, S. S. Pei, S. Hui, Appl. Phys. Lett. **59** (1991) 1864

[5] D. H. Zhang, W. Shi, P. H. Zhang, S. F. Yoon, X. Shi, Appl Phys Lett, **74** (1999)1570-1572
[6] D. H. Zhang, W. Shi, N. Li, Juanhao Chu, J Appl Phys, **92** (2002) 6287-6290
[7] R. People, J. C. Bean, C. G. Bethea, S. K. Sputz, L. J. Peticolas, Appl. Phys. Lett. **61** (1992)
1122
[8] R. P. G. Karunasiri, J. S. Park, K. L. Wang, Appl. Phys. Lett. **59**, 2588, 1991; **61** (1992) 2434

[9] P. Kruck, M. Helm, T. Fromherz, G. Bauer, J. F. Nutzel, G. Abstreiter, Appl. Phys. Lett. **69** (1996) 3372
[10] H. C. Liu, L. Li, M. Buchanan, Z. R. Wasilewski, G. J. Brown, F. Szmulowics, S. M. Hegde, J. Appl. Phys. **83** (1998) 585
[11] D. Krapf, B. Adoram, J. Shappir, A. Sa'ar, S. G. Thomas, J. L. Liu, K. L. Wang, Appl. Phys. Lett. **78** (2001) 495
[12] E. Corbin, K.B. Wong, M. Jaros, Phys. Rev. B **50** (1994) 2339
[13] I. Fromherz, E. Koppensteiner, M. Helm, G. Bauer, J.F. Nutzel, G. Abstreiter, Phys. Rev. **B 50** (1994)15073
[14] S. Ridene, K. Boujdaria, H. Bouchriha, G. Fishman, Phys. Rev. B **64** (2001) 085329
[15] D. Gershoni, C. H. Henry, G. A. Baraff, IEEE J. Quant. Electron. **29** (1993) 2433
[16] J-B. Xia, W-J. Fan, Phys. Rev. B **40** (1989) 8508
[17] S. T. Ng, W. J. Fan, Y. X. Dang, S. F. Yoon, Phys. Rev. B **72** (2005)115341
[18] S. L. Chuang, "*Physics of optoelectronic devices*", Wiley Series in pure and applied optics Edited by J. W. Goodman (1995)
[19] R. People, IEEE J. Quantum Electron. **QE22** (1986) 1696
[20] *Semiconductors, Physics Group IV Elements and III-V Compounds*, edited by O. Madelung,
M. Schultz, and H. Weiss, Landolt-Bo¨rnstein, New Series Group III, Vol. 17, Springer-Verlag, New York (1982)